



Comparison of water vapour products retrieved from Metop-A by Radio Occultation, Infrared and Microwave systems

Vinícius Ludwig-Barbosa¹, Johannes Kristoffer Nielsen¹, Kent Bækgaard Lauritsen¹, Brian Kerridge^{2,3}, Richard Siddans^{2,3}, and Tim Trent^{4,5}

Correspondence: Vinícius Ludwig-Barbosa (viba@dmi.dk)

Abstract. Water vapour (WV) is an essential climate variable (ECV) and different Earth Observing Systems (EOS) have been used to monitor and characterise its distribution, transportation and interplay in different phenomena. Metop-A satellite carried since 2006 four of such systems: (i) Infrared Atmospheric Sounding Interferometer (IASI), (ii) Advanced Microwave Sounding Unit (AMSU-A), (iii) Microwave Humidity Sounder (MHS), and (iv) Global navigation satellite system Receiver for Atmospheric Sounding (GRAS) performing radio occultation (RO) measurements. These systems operate at different frequencies, with different acquisition geometries, and also use different retrieval schemes to obtain vertically resolved WV profiles in the troposphere. Therefore, they provide independent measurements of WV, each with its limitations and strengths. Their characterisation via comparison with other data sets is important to estimate their systematic differences and uncertainties, which must be known when it comes to their use as climate data records (CDR) in climate monitoring and change studies. In this study, the water vapour product part of the Rutherford Appleton Laboratory (RAL) Infrared and Microwave System (IMS) scheme used in the European Space Agency (ESA) Water Vapour Climate Change Initiative (WV_cci) is compared to GRAS-RO WV data, part of Radio Occultation Meteorology Satellite Application Facility (ROM SAF) CDR, v1.0. The comparison uses ERA-Interim analysis and the Global Climate Observing System (GCOS) Reference Upper-Air Network (GRUAN) as references and presents the systematic differences in different latitude bands, gauges the influence of cloud contamination on the statistics, as well as the differences between profiles over land and water, and during day- and nighttime. Results in the lower troposphere (LT) show a significant difference between the data sets, where RAL IMS is wetter than ERA-I and GRUAN, especially in mid and high latitudes and over water (up to 14% ppmv) regardless of clouds, whereas GRAS-RO is drier than the references (5.3% ppmv at maximum w.r.t. GRUAN and during night). In the upper troposphere (UT), both data sets are drier than ERA-I (16.8% ppmv, RAL IMS; 7.2% ppmv, RO) and wetter than GRUAN (up to about 20% ppmv). In terms of variability, smoothing GRAS-RO, ERA-I and GRUAN with RAL IMS WV averaging kernels (AK) reduces the magnitude of their median absolute deviation (MAD) and increases their similarities (LT: RO, 8.78% ppmv; RAL IMS, 12.75% ppmv. UT: up to 36.33% ppmv).

¹National Centre for Climate Research, Danish Meteorological Institute, Copenhagen, Denmark

²Remote Sensing Group, STFC Rutherford Appleton Laboratory, Chilton, United Kingdom

³National Centre for Earth Observation, STFC Rutherford Appleton Laboratory, Chilton, United Kingdom

⁴Earth Observation Science, School of Physics and Astronomy, University of Leicester, Leicester, UK

⁵National Centre for Earth Observation, School of Physics and Astronomy, University of Leicester, Leicester, UK





1 Introduction

Water vapour (WV) is a greenhouse gas and an essential climate variable (ECV), and being able to characterise its distribution in the atmosphere as well as its transport mechanisms is an important aspect of detecting and tracking patterns connected to climate variability and change (Bojinski et al., 2014). For this purpose, a vast number of sensors have been applied to provide a long record of tropospheric water vapour in the most accurate and precise form, which is a burdensome task given its drastically varying concentration both with (i) altitude, where it decays nearly as an exponential function from the surface towards the upper troposphere, and (ii) along latitudes – from large amounts in the warm tropics to much smaller ones in the cold high latitudes (Sherwood et al., 2010).

Among the most relevant and long-term alternatives to measure water vapour are radiosondes (RS) (Seidel et al., 2009) and Earth Observing Systems (EOS) (Schröder et al., 2018), e.g., nadir sounders (microwave, MW; infrared, IR) and Global Navigation Satellite System (GNSS) Radio Occultation (RO) receivers (Li et al., 2000; Hilton et al., 2012; Kursinski et al., 1997).

All techniques have their merits but also caveats. Global Climate Observing System (GCOS) Reference Upper-Air Network (GRUAN) has a growing list of certified sites providing quality WV vertical profiles with traceable estimate of their uncertainties (Bodeker et al., 2016) and resolution of about 5-10 m, but its data requires corrections, e.g., to attenuate dry bias during daytime due to solar radiation (Miloshevich et al., 2006; Vömel et al., 2007; Dirksen et al., 2014); sites are coarsely distributed; do not cover oceans and; are highly concentrated in the north hemisphere.

Instruments onboard the Low Earth Orbit (LEO) satellites, such as the ones part of the Meteorological Operational (Metop) satellite programme operated by the European Organisation for the Exploitation of Meteorological Satellites (EUMETSAT), have the benefit of providing global coverage (Klaes et al., 2021). Advanced Microwave Sounding Unit (AMSU)-A and Infrared Atmospheric Sounding Interferometer (IASI) deliver WV profiles with 2-km vertical resolution at best and sampled along and across tracks in a resolution of 48 km and 25 km, respectively (Li et al., 2000; Hilton et al., 2012). The coarser vertical resolution compared to GRUAN limits to some extent the complete representation of the vertical WV variability, on top of suffering from cloud contamination, which degrades the measurement accuracy within and below clouds (Susskind et al., 2003, 2006).

GNSS-RO is an all-weather limb-sounding technique which scans different layers of the atmosphere, including the troposphere, and measures, first and foremost, refractivity profiles after the excess phase and precise time and velocities of GNSS and LEO satellites (Kursinski et al., 1997). In the lower troposphere (LT), GNSS-RO vertical profiles can achieve resolutions of 100-500 m, but their horizontal resolution is up to 300 km (Rocken et al., 1997). Also, its capability to retrieve water vapour data is directly related to the WV contribution to refractivity, and to do so, it requires a priori information to disentangle the wet from the dry share by applying an optimal estimation method such as the one-dimensional variational (1D-Var) method (Healy and Eyre, 2000).

RO WV data from different processing centres have been extensively compared to data sets provided by radiosondes, MW and IR systems, and climate models for complete characterisation. Ho et al. (2010) compared early University Corporation for Atmospheric Research (UCAR) 1D-Var COSMIC WV profiles to three sorts of radiosondes in four sites, and to ECMWF





analysis over four months in 2006. RO tended to be slightly drier than ECMWF (0.2 g/kg in LT) and confirmed differences between RS biases during day and night. The analysis was extended in Wang et al. (2013) by collocating a 4-year RO WV data set to 737 RS (8 types) part of the Integrated Global Radiosonde Archive (IGRA). It showed a global RO average dry bias (0.012±0.666 g/kg) from 200 to 925hPa and moving towards wet with altitude. Another 4-year study compared three different RO missions, and GRUAN (RS90/92) WV profiles and showed an overall RO dry bias up to mid-troposphere (400 hPa), and moist above (Ladstädter et al., 2015). In a comparison across centrers, therein UCAR, Wegener Center for Climate and Global Change (WEGC) and Radio Occultation Meteorology Satellite Application Facility (ROM SAF), results agreed on accuracy and precision to 10 INGRA's sondes where RO WV profiles were drier than the RS in the LT and lower mid-troposphere, and moister in altitude above about 600 hPa (about 15% at 300 hPa) with standard deviation up to 30% (Li et al., 2020). More recently, COSMIC-2 WV data processed by the National Oceanic and Atmospheric Administration (NOAA) Centre for Satellite Applications and Research (STAR) also showed a RO dry bias (0.26 g/kg ± 1.05 g/kg) in the LT and a slightly moist bias in the mid and upper troposphere compared to Vaisala RS41 (Ho et al., 2022).

In comparison studies to MW and IR, a 9-year data set of UCAR COSMIC 1D-Var WV profiles showed (i) a relatively dry bias compared to European Centre for Medium-range Weather Forecast (ECMWF) Reanalysis Interim (ERA-Interim) in $\pm 40^{\circ}$ latitude and between 400 and 700 hPa, and (ii) agreement up to 600 hPa and wet bias to AIRS above 600 hPa (Vergados et al., 2018). In Rieckh et al. (2018), the spatial differences of WV RO data provided by three processing centres (UCAR, JPL, WEGC) were compared to AIRS data in the tropics and sub-tropics in 2017, and used ERA-Interim as the reference. Results showed that RO 1D-Var WV profiles from different centres were, on average, drier than ERA-Interim between 1000–400 hPa, and wetter and more precise than AIRS in the same range. None of the comparison studies, including MW or IR data, investigated the influence of cloud contamination.

A common practice to improve the quality of retrieved WV profiles is combining data from different sensors to improve the vertical resolution, reduce the uncertainties at specific regions and the influence of clouds. In the early days of RO, Von Engeln et al. (2001) tested combining RO with MW to retrieve "dry" temperature profiles from the surface up to 90 km using an optimal estimation method (OEM) scheme. Another approach using multivariable regression combined AIRS radiances to RO refractivity and increased the amount of independent information available at specific layers of temperature and humidity retrievals in LT, and achieved a significant improvement in root mean squared error (RMSE) compared to the results achieved with independent retrievals (Ho et al., 2007). These results agree with findings below 700 hPa reported in Liu et al. (2016), where a 1D-Var approach combining COSMIC refractivity and AIRS radiance was applied and compared to ERA-Interim. Similarly, simulated and real data over the ocean from COSMIC-2 (bending angles) and Advanced Technology Microwave Sounder (ATMS) on Suomi-NPP (National Polar-orbiting Partnership) (brightness temperatures) were combined in the 1D-Var retrieval, achieving a remarkable reduction of vapour pressure dry biases, compared to RO-alone, within the planetary boundary layer (PBL) for cases affected by ducting triggered by marine stratocumulus clouds (Wang et al., 2024). In contrast to 1D-Var and OEM, Vergados et al. (2014) assumed a simpler approach to assess the particular case of WV retrieval in cloudy regions by combining collocated COSMIC refractivity and AIRS temperature profiles into the Smith-Weintraub equation (Kursinski





et al., 1997). Results showed less dry biases below 700 hPa in the tropics and high latitudes compared to rawinsondes than AIRS-alone.

In this study, WV vertical profiles from ROM SAF climate data record (CDR), v1.0 (ROM SAF, 2019; Gleisner et al., 2020), are compared to the Rutherford Appleton Laboratory (RAL) Infrared and Microwave Sounding (IMS), v2.1, data set – a 9.5-year CDR based on a joint retrieval of IASI, AMSU-A and Microwave Humidity Sounder (MHS) data given by an OEM scheme, which was developed originally in a study for EUMETSAT (Siddans et al., 2015), subsequently developed through UK NCEO and applied during the European Space Agency (ESA) Water Vapour Climate Change Initiative (WV_cci) project (Siddans et al., 2018; Siddans, 2023).

This comparison aims to map differences among the collocated WV data captured by this suite of sensors on board Metop-A between June 2007 and December 2016. The comparison uses ERA-Interim analysis and GRUAN sondes as references. It also investigates the influence of clouds, geographical location, i.e., profiles over land and sea, and time of day. It extends the assessment reported in Trent et al. (2023), in which compared to GRUAN data, (i) RAL IMS showed a dry bias in the low and mid troposphere, and a larger wet bias in the upper troposphere (up to 10% ppmv); (ii) RAL IMS daytime dry biases were significantly larger than during nighttime between 850 and 1000 hPa, whereas nighttime dry biases were predominant above 700 hPa, and (iii) RAL IMS showed wet biases in LT which expanded to mid troposphere (MT) in profiles with larger cloud fraction during daytime than in all matchups, whereas dry biases were observed regardless of cloud cover in the upper troposphere. The biases are inverted during nighttime and otherwise follow the same relationship to cloud fraction.

The remainder of this document is presented as follows: Sect. 2 provides details about the data sets, Sect. 3 addresses the matchup criteria, quality control and the approach to attenuate the difference in measurements' footprints, i.e., averaging kernel (AK) filtering. Finally, the results are presented in Sect. 4 and conclusions are given in Sect. 5.

2 Data

115

2.1 RAL IMS data

The Infrared Microwave Sounding (IMS) scheme employs the optimal estimation method (OEM) to jointly retrieve atmospheric and surface parameters from operational sounding instruments.

The scheme retrieves water vapour, temperature, ozone profiles, surface spectral emissivity, and cloud parameters jointly from the Metop sounding instruments IASI, MHS and AMSU. Surface pressure, initial guess temperature, water vapour profiles, and wind speed (for surface reflectance) are specified by ERA-5, and in the near-real time implementation by the ECMWF Integrated Forecast System (IFS). The *a priori* water vapour profiles for this optimal estimation scheme are from a zonal mean climatology with fractional uncertainties larger than 80% in the troposphere and, therefore, independent of ECMWF forecasts or analyses such as ERA-Interim.

The IMS scheme and its validation against GRUAN and ARSA radiosondes is described in Trent et al. (2023) and in greater detail in the Algorithm Theoretical Basis Document, ATBD (Siddans, 2023). The RAL IMS data set used in this comparison spans from June 2007 to December 2016 (Siddans et al., 2018).





Recently, the scheme has also been applied to process the full periods of both the Metop series (2007-2025) and Suomi-NPP/NOAA-20 (2012-25) missions to date. In this current extended version, column retrieval of several additional minor trace gases and two types of aerosol (dust and volcanic sulphate) are included in the data set. The scheme has been adapted and applied to the CrIS and ATMS sounders onboard Suomi-NPP and NOAA-20 as well.

2.2 ROM SAF data

150

This section provides an overview of the one-dimensional variational (1D-Var) algorithm used to retrieve WV profiles from RO measurements. The radio occultation data evaluated in this paper are a product of measurements recorded by the GPS Receiver for Atmospheric Sounding (GRAS) instrument onboard Metop-A, covering the years 2007 to 2016. The GRAS data were processed as part of ROM SAF Reprocessing v1.0 and composed the ROM SAF Level 2 product (ROM SAF, 2019; Gleisner et al., 2020).

2.2.1 Radio Occultation 1D-Var configuration

The ROM SAF water vapour climate data record (ROM SAF CDR v1.0) was produced by a 1D-Var algorithm described in the ATBD (ROM SAF, 2021), available at the ROM SAF's website. The RO processing utilises the Radio Occultation Processing Package, ROPP (Culverwell et al., 2015), and all RO profiles were subject to the ROM SAF quality control (Steiner et al., 2020). The 1D-Var retrieval was performed using ECMWF Reanalysis Interim (ERA-Interim) forecast (fc) temperature and specific humidity profiles, and surface pressure as background (Dee et al., 2011). The 1D-Var state vector was defined in the framework of the ERA-Interim hydrostatic model level structure. In this setup, the state of an air column is determined by temperature and specific humidity on 60 hybrid model levels, as well as surface pressure.

ERA-Interim forecast profiles and surface pressure were fetched from the ECMWF MARS archive on a $1^{\circ} \times 1^{\circ}$ latitude-longitude grid with 6-hourly time steps. For each occultation, an individual background profile was interpolated from two consecutive forecasts at the occultation reference coordinate. The forecasts were chosen for each occultation so that the model runs, from which they were derived, were independent of the particular occultation.

The assumed error covariance matrices of the input vectors determine the performance of 1D-Var. The error covariance matrix of the observational (refractivity) vector was constructed with a standard deviation of 2% in the troposphere, and with a vertical correlation length of 3 km. A latitude-dependent background ERA-Interim error covariance matrix was calculated from disseminated ERA-Interim uncertainty estimates provided by ECMWF (Holm and Kral, 2012).

The temperature and specific humidity averaging kernels (AK) for the ROM SAF 1D-Var are presented in Fig. 1 along with their respective cumulative degrees of freedom for the signals (CDOFS), which correspond to the trace of the AK matrix.

The AKs are plotted in Fig. 1(a) such that each curve corresponds to a row of the AK matrix. Thus, each curve shows the sensitivity of one specific component of the humidity solution to deviations from the background at all pressures. At mid latitudes the AKs indicate a good sensitivity between 900 and 300 hPa. Figure 1(b) illustrates the same by showing the solution uncertainty divided by the background uncertainty and highlights the regions where most information is provided by the measurement, i.e., where the fraction $\frac{\sigma_s}{\sigma_b}$ is at lowest. From the CDOFS in low latitudes ($\pm 30^{\circ}$), and mid latitudes



160



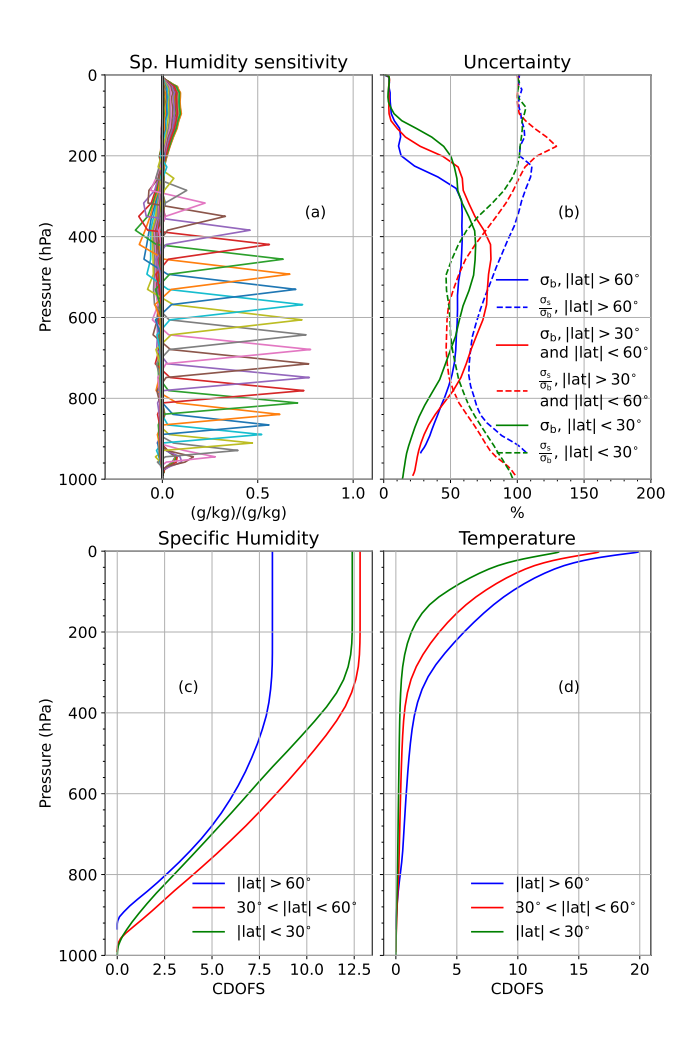


Figure 1. Performance indicators of the ROM SAF CDR v1.0 1D-Var, calculated as means over Metop-A profiles from 1 October 2007. From the left: (a) Rows of Averaging Kernels (AKs) for specific humidity at mid latitudes, (b) uncertainty of background specific humidity (full curves) and 1D-Var solution specific humidity uncertainty divided by background uncertainty, (c) cumulative degrees of freedom in the signal (CDOFS) for specific humidity and (d) CDOFS for temperature. In panels (b), (c) and (d) each curve represents a latitude band (see legends).

 $(\pm 30^{\circ}-60^{\circ})$, it can be seen that Metop-A RO measurements have around 12 to 13 independent degrees of freedom in the retrieval of mid latitude tropospheric WV, whereas 7 to 8 degrees of freedom are obtained at high latitudes $(\pm 60^{\circ}-90^{\circ})$. The RO WV product is a representation of the water vapour contribution in refractivity (Kursinski et al., 1997; Ho et al., 2022), and the CDOFS figures are illustrative to indicate the maximum altitude where water vapour information is available in RO measurements, i.e., where the gradient in the CDOFS curves tends to zero. In the tropics there is sensitivity up to a height corresponding to 200 hPa. In polar regions the maximal height is close to 300 hPa.





2.3 ERA-Interim

Besides ERA-Interim forecast profiles, ERA-Interim analysis had also its fields interpolated at the closest point in space and time to every occultation reference point (ROM SAF, 2021). ERA-Interim analysis profiles are used as one of the reference data sets for the comparison between RAL IMS and RO WV data.

Among different satellites and in-situ data, brightness temperature (temperature) from AMSU-A, humidity profiles from MHS and bending angles from GRAS-RO (Metop-A) were assimilated into ERA-Interim. However, RO was not the remote sensing technique with the largest share of data assimilated – satellite radiances were. The GRAS-RO instrument was 1 out of 10 receivers with data assimilated by ERA-Interim – COSMIC had the largest share. Thus, using ERA-Interim as the reference in the context of this study is still reasonable. Nevertheless, the assimilation of RO data had the following impacts on the ERA-Interim water vapour data: (i) over ocean, drying effect below 800 hPa and moistening around 800 hPa and; (ii) over land, moistening around 600 hPa (Poli et al., 2010).

The ERA-Interim profiles initially available in 60 levels were further interpolated using cubic spline into RTTOV 101 pressure levels and converted from mass mixing ratio (g/kg) to volume mixing ratio (ppmv), see Appendix A. Hereafter, ERA-Interim analysis (an) data is referred to as ERA-I.

2.4 GRUAN WV data

The RS92-GDP.2 data set, provided by the GCOS Reference Upper-Air Network, GRUAN, (Sommer et al., 2012; Dirksen et al., 2014), contains relative humidity (RH) profiles measured by the Vaisala RS92 radiosonde. Established as a long-term provider of fiducial measurements, this data set was considered along with ERA-I as a reference for comparing RAL IMS and RO WV data. Information about 16 GRUAN stations whose data were used in this comparison is available in Appendix C. GRUAN data is sampled in intervals of 2 s resulting in high-resolution vertical profiles (5-10 m) with variable pressure levels among measurements. Therefore, GRUAN RH profiles collocated to RAL IMS and RO, i.e., triplets rather than pairs, were interpolated using cubic spline to the fixed RTTOV 101 pressure levels, and converted to volume mixing ratio – see Appendix B.

3 Methodology

180

185

The comparison is based on a data set of matchups, built following a specific collocation criteria, quality control (QC) checks, and subject to interpolation and filtering to equalise profiles to the same pressure levels and reduce their footprint differences.

3.1 Collocation

The search for collocations assumed the spatial constraint of 300 km and temporal constraint of 3 hours between matchups. The spatial criterion differs from the one adopted in Trent et al. (2023) due to the RO geometry and the motion of the LEO satellite during one occultation event, which results in a larger measurement footprint than in a nadir-based system, up to \sim 300 km





compared to 48 km (Rocken et al., 1997; Hilton et al., 2012). Collocation between a pair of measurements was determined by (Meredith et al., 2023)

$$|t_A - t_B| < \Delta_t, \tag{1}$$

$$\sqrt{(\lambda_A - \lambda_B)^2 \cos^2 \theta_B + (\theta_A - \theta_B)^2} < \Delta d / R_E, \tag{2}$$

where λ and θ are longitudes and latitudes in radians for measurements A and B, R_E is the Earth's radius, t is time of the measurement acquisition, and Δd and Δt are the spatial and temporal constraints.

For the search in time, the entire interval of the occultation event was compared to different scenes/pixels in the MW/IR swath. For the spatial search, the RO reference coordinates of the occultation events – located approximately in the upper troposphere (UT) – were compared to the coordinate of the scenes in the nadir sounder swath. Since all systems are onboard Metop-A and given their particular geometries, the interval of possible collocation along the same satellite track and its first adjacent is centred around ± 8 and ± 100 minutes (Ladstädter, 2012). Limiting the search to these time intervals significantly reduces the number of pairs to be checked.

Besides satisfying (1) and (2), RAL IMS and RO (ERA-I) WV profiles followed an extra requirement that the difference in the highest point in pressure (lowest in altitudes) differs by 10 hPa (~100 meters) at most. This constraint avoids collocations where one of the profiles could be located, e.g., in a mountain range, whereas its potential matchup could be at sea level. For RAL IMS data, the lowest point on the profiles is set either by the GTOPO30 model or the interpolated NWP surface altitude (Siddans, 2023).

210 3.2 Quality Control, Interpolation and Filtering

After matchups were established, quality control was performed in WV profiles considered in the analysis, and further steps were made to keep the coherence between profiles from the different data sets, i.e., interpolation to common pressure levels and filtering.

3.2.1 RAL IMS data

RAL IMS retrieval applies the OEM scheme, and WV profiles have been considered in the comparison only when the cost function was satisfied, herein $j_x + j_y < 1000$, where j_x is the state vector component and j_y stands for the measurement component (Siddans, 2023). Inherently, only RAL IMS profiles in which the OEM algorithm converged were assessed.

Next, pressure levels where the WV uncertainty was larger than 50% have been set to not-a-number (NaN). Further, the criterion of cloud fraction lower than 80%, assumed in Trent et al. (2023), was also adopted as a baseline in this study to limit cloud contamination. Finally, only RAL IMS WV profiles with available averaging kernels (AK) composed the data set of matchups.



225

230

235

245

250



3.2.2 Averaging Kernel Filtering

As aforementioned, averaging kernels characterise the sensitivity in the retrieved profile (state) to changes in the quantity (true state) in different layers (Rodgers and Connor, 2003). As seen in Fig. 1, AKs also indicate the vertical resolution achieved in the retrieved profiles, which is dependent on the remote sensing technique geometry, operating frequencies, and the assumptions in a particular retrieval method, e.g., error covariances, forward model, etc..

In comparison studies between data sets provided by different remote sensing techniques, an important step is performing vertical smearing to achieve a common vertical resolution, e.g., using a low-pass or boxcar filter (Kuo et al., 2004; Feltz et al., 2014; Gilpin et al., 2018). Alternatively, AKs offer a possibility to equalise the differences in footprint by convolving the high-resolution profile with the AKs of the collocated low-resolution profile. The estimated resolution for RAL IMS WV profiles based on the CDOFS of their AKs is 2 km at best (Siddans, 2023; Trent et al., 2023). Therefore, RAL IMS AKs and profiles of other data sets are convolved (Trent et al., 2023),

$$\ln(x_{\text{est}}) = \ln(x_{\text{IMS,ap}}) + \mathbf{AK_{\text{IMS}}} \times \ln\left(\frac{x_0}{x_{\text{IMS,ap}}}\right),\tag{3}$$

where $\mathbf{A}\mathbf{K}_{\mathrm{IMS}}$ is the RAL IMS AK 101-level square matrix, x_0 is the water vapour profile (in volume mixing ratio, ppmv) to be convolved, i.e., GRAS-RO, ERA-I or GRUAN, $x_{\mathrm{IMS,ap}}$ is the IMS WV a priori profile, and x_{est} is the resulting convolved WV profile. As a quality control step, RAL IMS profiles whose $\max(\sum_{j=1}^{101}\mathbf{A}\mathbf{K}_{ij}) > 2$ or $\min(\sum_{j=1}^{101}\mathbf{A}\mathbf{K}_{ij}) < -1$ were not considered in the comparison, since applying their AKs in (3) resulted in smoothed profiles showing unrealistically large values.

Unavailable levels at the top or bottom of RO, ERA-I or GRUAN profiles were set to a constant, equal to the nearest available value, to avoid the eventual disparity in levels with their RAL IMS matchaps before the convolution. Then, values in the convolved profiles were removed at the levels filled with constants were not part of the comparison.

Particularly to the methodology including AK filtering, a given RO and GRUAN profile is most likely collocated to n scenes in the IASI-AMSU-MHS swath. Since the RAL IMS profiles have slightly different AKs, the AK filtering will result in n smoothed copies of the RO and GRUAN profiles. Since all copies are averaged during the statistics computation, the copies did not create any problem in the analysis. Figure 2 shows an RAL IMS WV AK matrix and difference between original and smoothed profiles.

The AKs can also be used to assess the amount of information originating from the measurement and the background in a retrieved profile. Such an assessment is done by the sum of the AK matrix columns, i.e., the area of the kernels. Values close to unity indicate the predominance of the measurement's information rather than the background, and the contrary when the sum is closer to zero (Rodgers and Connor, 2003). In Fig. 2(a), the black dashed line indicates that the measurement provided most of the information in the retrieval up to about 300 hPa.





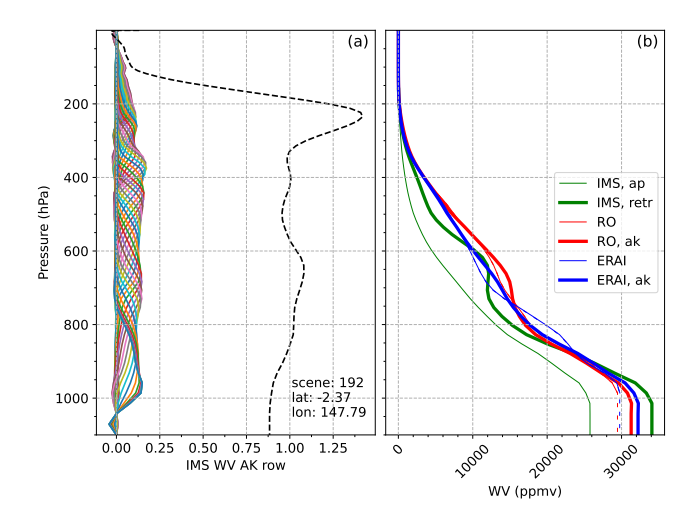


Figure 2. Averaging kernel filtering. Panel (a) shows the rows of one RAL IMS WV AK matrix, where each curve corresponds to the sensitivity at a specific level, and the dashed curve shows the sum of AK matrix rows. Panel (b) shows a comparison between the original and AK-smoothed profiles. Thin lines represent RAL IMS a priori (green), RO (red) and ERA-I (blue) original profiles. Dashed lines illustrate the levels filled with constant values. Thick lines show the RAL IMS retrieved WV profile, and RO and ERA-I filtered profiles following the same colour pattern. Statistics assuming filtered profiles do not consider the levels where constants were added to the original profiles. RAL IMS file: 20140227231756z_20140228005955z_150_199, RO level 2, wet file: 20140227_220451_META_G002_R_2305_0010.

3.2.3 ROM SAF WV data

The RO WV water vapour profiles collocated to RAL IMS profiles are considered in the analysis depending on the ROM SAF's PCD flag, which labels the 1D-Var retrieved WV profiles into "nominal" and "non-nominal" (ROM SAF, 2024). Hereafter, only "nominal" profiles were considered.

Negative values in the profiles are replaced by an infinitesimal positive value to avoid problems in the conversion from mass mixing ratio (specific humidity, in g/kg) to volume mixing ratio (ppmv), see Appendix A. Then, RO WV profiles originally disseminated in 60 levels were interpolated, using the spline method, to the RTTOV 101 levels. Lastly, values at pressure levels where the collocated RAL IMS profiles did not meet the uncertainty criteria were also not part of the analyses.

260 4 Results

265

In this section, an analysis of collocated cases in the matchup database using robust statistics, i.e., the median and median absolute deviation (MAD), is presented. Results are split between the two reference (ERA-Interim and GRUAN) and present the initial comparisons for cases in the matchup database. These results are broken down further by considering the influence of cloud parameters, land and ocean surfaces, and separation into day & night scenes on profile biases. With water vapour concentrations varying by four orders of magnitude between the surface and the tropopause, this study adopts the convention





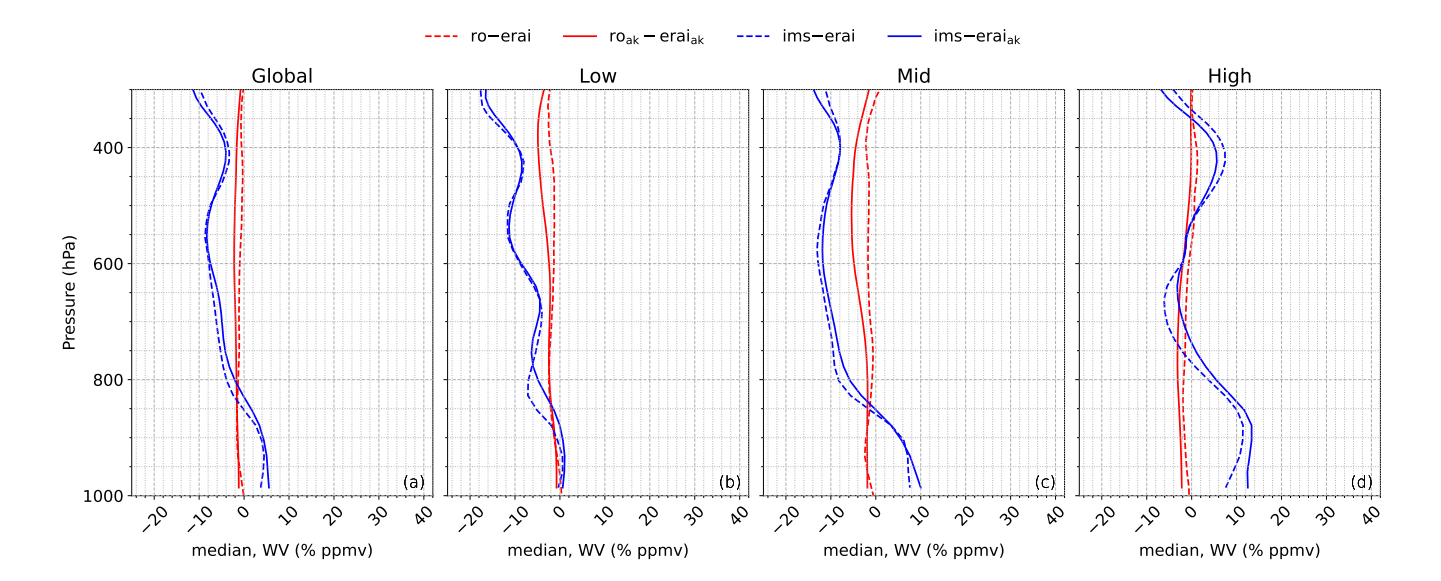


Figure 3. Median differences of RO and IMS profiles to ERA-Interim analysis WV profiles in (a) global, (b) low-, (c) mid- and (d) high-latitude statistics. Dashed lines represent statistics based on original RO and ERA-I profiles, and solid lines represent statistics for profiles convoluted by RAL IMS AKs. RO AK-smoothed profiles were subject to the same truncation as their RAL IMS matchups. Only RAL IMS profiles with cloud fraction up to 80% (baseline) are considered.

used in Trent et al. (2023) and presents results as a percentage of volume mixing ratio (% ppmv). Supplementary material is provided to allow the conversion from relative values to ppmv, as well as to specific humidity (see Appendix A).

4.1 Comparisons against ERA-Interim

275

280

Firstly, RAL IMS and GRAS-RO WV profiles are compared against ERA-I. As mentioned in Sect. 2.3, for the ROM SAF product, though the forecasts are used as the background to the 1D-Var scheme and GPS-RO observations are assimilated into ERA-I, we consider there is sufficient independence between the collocated cases, as information content will be dominated by other sources (e.g., COSMIC, Aqua, MW and IR). Figure 3 shows median differences based on RO and ERA-I WV profiles interpolated to RTTOV 101 pressure levels, and on their AK-smoothed versions.

The differences between the RO and RAL IMS WV profiles can be divided into two regions: the lower troposphere (1000–850 hPa), and the mid and upper troposphere (850–300 hPa). Globally and in the upper region, RAL IMS and RO data are drier than ERA-I. RAL IMS is drier than RO – 11.37% and 2.21% ppmv, respectively. The dry tendency in RAL IMS mostly comes from low and mid latitudes profiles, 3.10 to 16.54% ppmv drier than ERA-I. The statistics in high latitudes deviate from this pattern for RAL IMS profiles between 350–500 hPa, where they tend to be wetter than ERA-I (5.60% ppmv). In regards to RO, the largest difference to ERA-I is observed in mid latitude, 5.39% ppmv in mid troposphere.

Globally and at the lower region, RAL IMS becomes wetter than ERA-I (5.54% ppmv), whereas RO is consistently drier. The wet tendency in RAL IMS data is mainly driven by mid- and high-latitude profiles – 10% and 13.34% ppmv, respectively.



285

295

305



Convolving RO and ERA-I profiles with RAL IMS AKs yields drier profiles than their originals, as indicated by the median differences. RAL IMS statistics compared to AK-smoothed ERA-I (solid blue) are slightly moister than compared to statistics assuming non-smoothed ERA-I profiles in most levels. RO statistics assuming AK-smoothed profiles are drier than those with non-smoothed profiles. These results indicate convolving WV profiles with RAL IMS AKs yields drier profiles, especially in data sets with higher vertical resolution. For instance, GRUAN smoothed profiles becomes relatively drier than RO smoothed profiles w.r.t their originals.

Overall, the ROM SAF WV dry bias relative to ERA-I is consistent with previous comparisons that used different retrieval algorithms and RO missions (Rieckh et al., 2018; Vergados et al., 2018).

290 4.1.1 Influence of clouds

Next, the influence of cloud parameters was investigated to identify the origin of different biases in RAL IMS and RO WV data. In Trent et al. (2023), the baseline criterion for cloud parameters in RAL IMS collocated profiles was cloud fraction up to 80% (CC1), without considering cloud top height. In this study, three additional sets of criteria were evaluated, aiming at more restrictive selections of RAL IMS WV profiles:

- CC2: Cloud fraction up to 5%,
- CC3: Cloud fraction up to 30% and cloud top height up to 3 km,
- CC4: CC2 or CC3 satisfied.

Results in global, low, mid, and high latitude regions for the four cloud parameter sets, and with and without averaging kernels filtering are shown in Fig. 4. Only RAL IMS statistics are shown, since RO measurements are less sensitive to cloud contamination (Rocken et al., 1997; Yang and Zou, 2012).

We observe that the different cloud parameter sets do not influence the wet tendency in the lower region of mid- and highlatitude profiles. In the upper region, the CC1 criterion selects profiles that tend to be moister than ERA-I; i.e., scenes with more cloud contamination and higher cloud cover result in a wet bias in RAL IMS WV data relative to ERA-I in high latitudes.

The remaining results presented in this section considered CC4 since the statistics of the combination of CC2 and CC3 do not diverge substantially from CC2 and CC3 alone, and the subset size is not as small as the one obtained with CC3 (see Table 1). Also, results are based on AK-smoothed profiles since there was no indication of significant differences in the statistics when using the original RO and ERA-I profiles.

4.1.2 Land & Water

Besides the influence of cloud parameters, profiles over land and water were split into two subsets to assess potential sources of biases. The data sets were separated using the package global-land-mask (Todd, 2020) with the requirement that both matched profiles must be over land or both over water. Figure 5 shows the median differences.





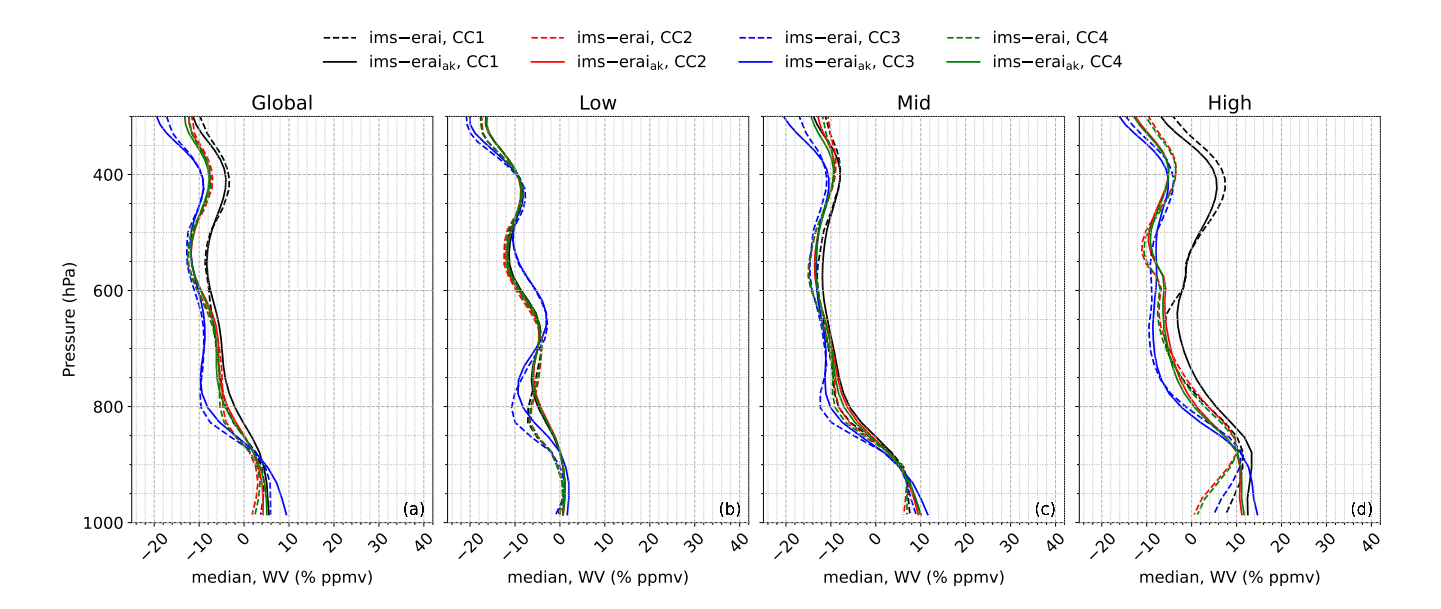


Figure 4. Median differences of RAL IMS profiles to ERA-Interim analysis WV profiles in (a) global, (b) low-, (c) mid- and (d) high-latitude statistics. Dashed lines represent statistics assuming original ERA-I profiles, and solid lines assume their AK-smoothed profiles as the reference. Black curves represent the statistics assuming the baseline cloud criterion (CC1), red curves are related to CC2, blue to CC3, and green to CC4.

Except for statistics in low latitudes, the RAL IMS wet biases compared to ERA-I are larger in the subset of profiles over water in mid and high latitudes (10.57% and 14.00% ppmv, respectively) than over land (3.87% and 4.39% ppmv, respectively) in LT. Further, the subset of profiles over water corresponds to most of the RAL IMS data set and, therefore, it accounts largely for the bias. Nevertheless, the RAL IMS wet bias is observed over land and water in LT. In UT, the driest difference to ERA-I is observed in low latitudes and in profiles over water (up to 16.81% ppmv).

Regarding RO averages, the most significant differences between over land and water subsets are observed in low and mid latitudes, in which the driest differences to ERA-I are observed in profiles over land (global, 2.84% ppmv; low latitude, 7.23% ppmv).

Table 1 summarises the number of profiles part of the statistics using ERA-I as the reference.

4.2 Comparisons against GRUAN

315

320

325

Figure 6 shows the median differences of RAL IMS and RO WV to GRUAN WV data.

Overall, the RAL IMS magnitudes of the median differences to GRUAN are similar to the ones reported in Trent et al. (2023). Globally, RAL IMS shows a wet bias of 2.76% ppmv in LT and up to 10% ppmv between 300–500 hPa. In both regions, the wettest biases are observed in high latitudes (LT, 12.40% ppmv; UT, 21.96% ppmv). RAL IMS and RO are remarkably similar for most of the mid troposphere, showing a slightly dry bias, up to 2.31% ppmv.





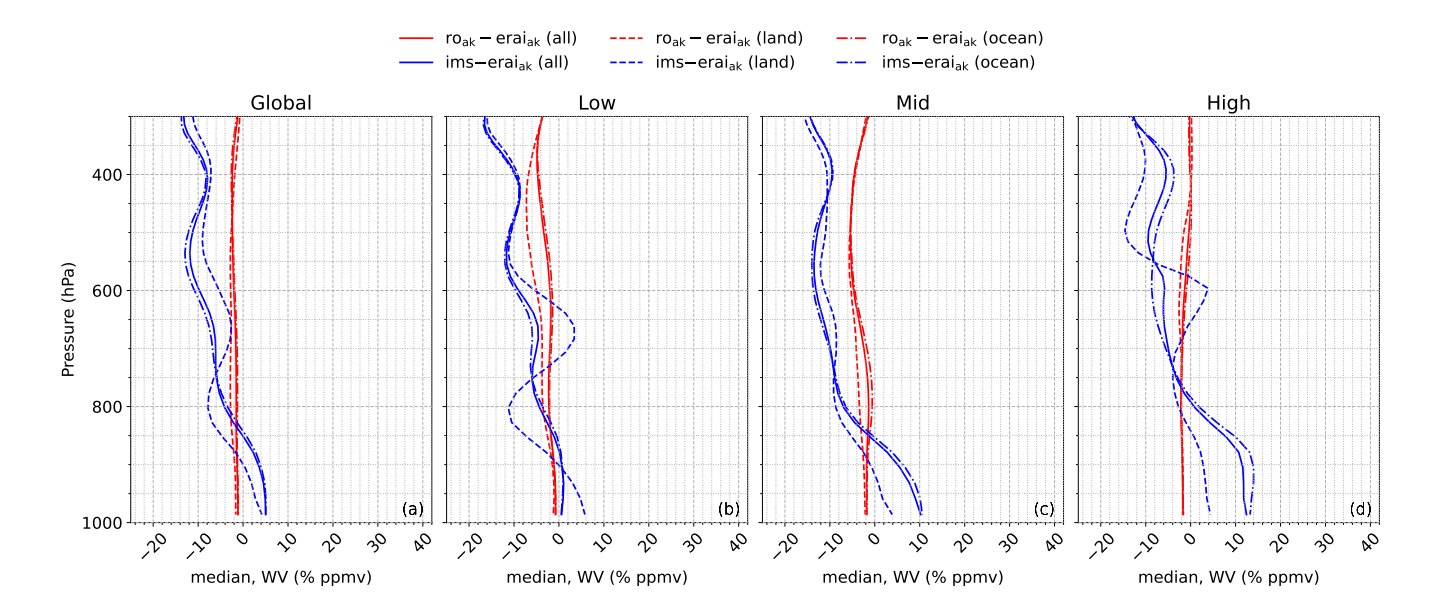


Figure 5. Median differences of RO and IMS profiles to ERA-Interim analysis WV profiles over land and water in (a) global, (b) low-, (c) mid-, and (d) high-latitude statistics. Solid lines correspond to combined statistics (land+water), dashed lines represent statistics over land, and dash-dotted lines represent statistics over water. RO and ERA-I profiles are AK-smoothed, and matchups follow CC4 criteria.

Table 1. Number of profiles part of the statistics using ERA-I as the reference. Numbers correspond to the largest number of points available at a given level, since they vary for different reasons – especially in the lower troposphere.

	Global	Low	Mid	High
RO	739,405	206,160	316,995	216,250
IMS	4,375,236	1,120,848	1,758,361	1,496,027
-, CC2	2,301,878	918,068	889,162	494,648
-, CC3	493,027	114,263	294,160	84,604
-, CC4	2,716,534	1,001,300	1,147,606	567,628
$-$, $CC4^L$	554,652	155,179	223,645	175,828
-, CC4 ^W	1,983,133	789,417	854,287	339,429

W = over water, L = over land

As in the analysis using ERA-I as the reference, RO data is slightly drier than GRUAN in LT (2.47% ppmv). The statistics in the different latitude bands indicate that RO tend to be moister than GRUAN in the mid and high latitudes in altitudes above 500 hPa (up to 22.98% ppmv in mid latitudes). In general, the results in different layers agree with the biases reported in similar studies (Ho et al., 2010; Wang et al., 2013; Ladstädter et al., 2015; Li et al., 2020).





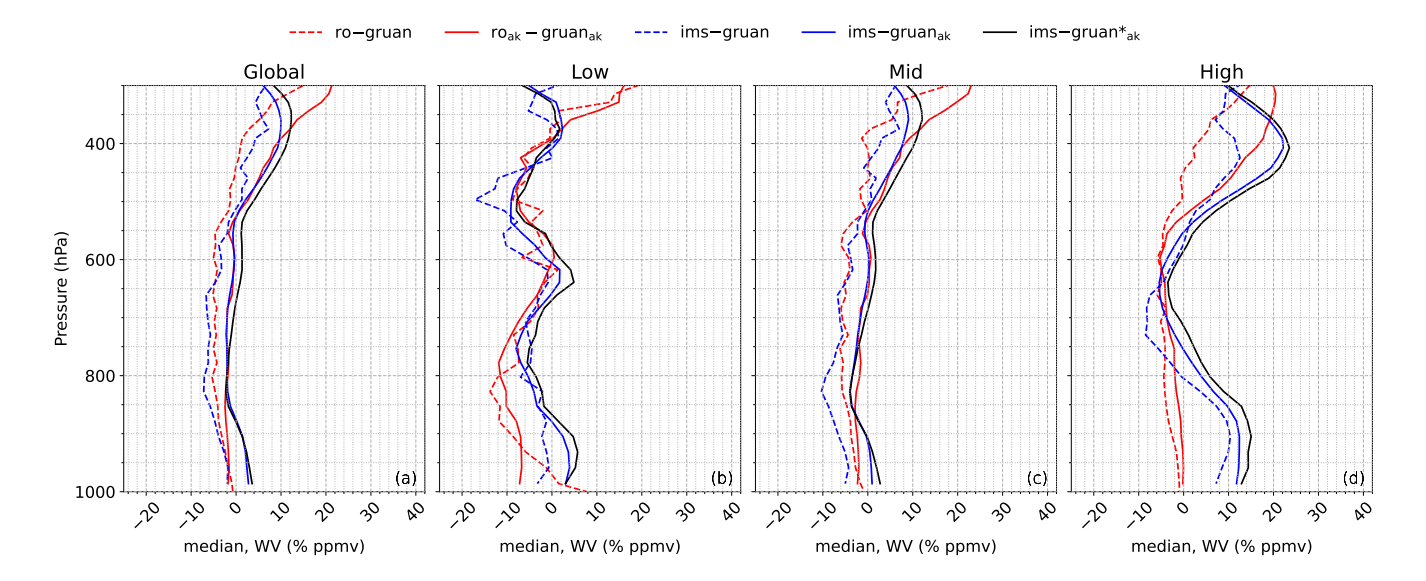


Figure 6. Median differences of RO and RAL IMS profiles to GRUAN WV profiles in (a) global, (b) low-, (c) mid-n and (d) high-latitude statistics. Dashed lines represent statistics based on original RO and ERA-I profiles, and solid lines represent their profiles convoluted by RAL IMS AKs. RO AK-smoothed profiles were subject to the same truncation as their RAL IMS matchups. Matchups follow CC1. Black curves labelled "ims-gruan*, ak" show the statistics for collocations no more than 100 km apart.

Regarding AK-smoothing, the median differences indicate that smoothed profiles are moister than those based on original profiles. Similar to the behaviour noticed in Fig. 3, GRUAN WV profiles have a higher vertical resolution than RO and, therefore, the GRUAN smoothed profiles compared to their originals are relatively drier than the RO smoothed ones compared to their originals.

A remark about the statistics in different latitude bands is the limited number of GRUAN sites in low latitudes (see Table 2), and generally in the southern hemisphere, as illustrated in Fig. C1. Therefore, statistics in low latitudes are the least reliable, and mid and high latitudes are predominantly a portrait of the northern hemisphere.

Figure 7 shows the MAD of differences.

335

The global MAD statistics for RAL IMS and RO are quite similar. RO data shows a slightly lower global MAD (between 8.78% and 12.75% ppmv) than RAL IMS (between 13.98% and 16.70% ppmv) in LT, even lower in high latitudes. In the mid and upper troposphere, the maximum MAD ranges between 14.75 and 36.33% ppmv for both data sets.

Regarding AK filtering, the results show a significant decrease in MAD when AK-smoothed profiles were assumed in statistics. It also equalised RAL IMS and RO variabilities compared to GRUAN in some levels.

The MAD magnitudes are larger, especially in LT and MT, than the ones reported in Trent et al. (2023), and the differences are due to the 300-km spatial criterion used here instead of the 100-km one considered by (Trent et al., 2023). The black curves in Fig. 6 and 7 correspond to the results obtained with the tighter spatial criterion. The maximum MAD ranges between 15.75% and 25% ppmv, smaller than observed in the 300-km criterion. The remaining difference to values reported in Trent





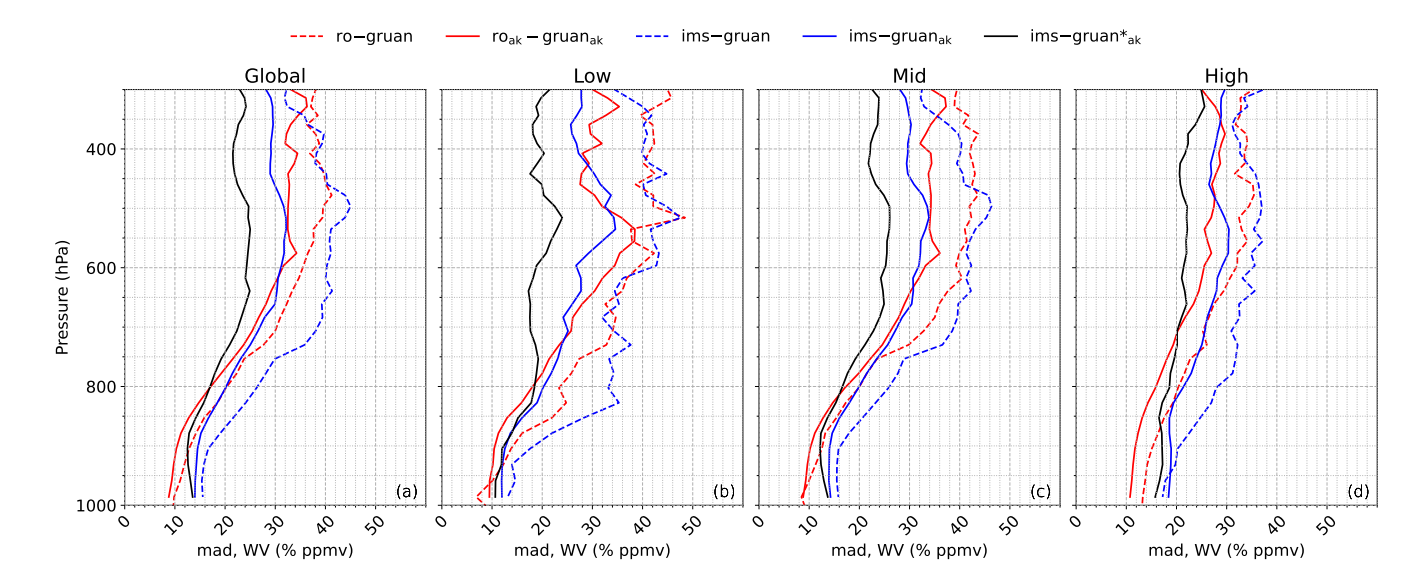


Figure 7. MAD of differences of RO and RAL IMS profiles to GRUAN WV profiles in (a) global, (b) low-, (c) mid-, and (d) high-latitude statistics. Dashed lines represent statistics based on original RO and ERA-I profiles, and solid lines represent their profiles convoluted by RAL IMS AKs. RO AK-smoothed profiles were subject to the same truncation as their RAL IMS matchups. Matchups follow CC1. Black curves labelled "ims—gruan*_{ak}" show the statistics for collocations no more than 100 km apart.

et al. (2023) may be due to the different computation of statistics, i.e., weighted averages within pressure layers. Regarding averages, different spatial criteria should not have an influence on the statistics if the distance between matchups is up to 600 km (Sun et al., 2010). The moister differences observed in the stricter collocations in Fig. 6 are related to the predominant sampling of clear sky scenes in the RAL IMS data set.

Day & Night

350

Figure 8 presents results for day and night subsets. As for the analysis in Sect. 4.1.2, all triplet members must have been acquired during day- or nighttime.

Most matchups are daytime profiles, which explains the similarity to the combined statistics (day+night). However, GRUAN nighttime profiles have lower uncertainties than daytime (Dirksen et al., 2014) and, therefore, remarks are based on nighttime subsets. In LT, RAL IMS is up to 3.78% ppmv wetter than GRUAN (global). The statistics indicate the bias is driven mainly by high-latitude profiles (16.92% ppmv), even though the wet bias is also observed in daytime profiles – a pattern not observed in Trent et al. (2023). RO is drier than GRUAN in LT, up to 4.64 (global) and 5.26% ppmv (high latitude). Both RO day- and nighttime follow this pattern in mid latitudes, but the daytime subset is slightly wetter than GRUAN in high latitudes.

In MT, RAL IMS and RO are drier than GRUAN up to about 600 hPa – 6.49% and 7.87% ppmv, respectively. Then, the bias flips and peaks at 22.54% ppmv in the RAL IMS set and 11.45% ppmv in the RO set. The driest profiles are observed in





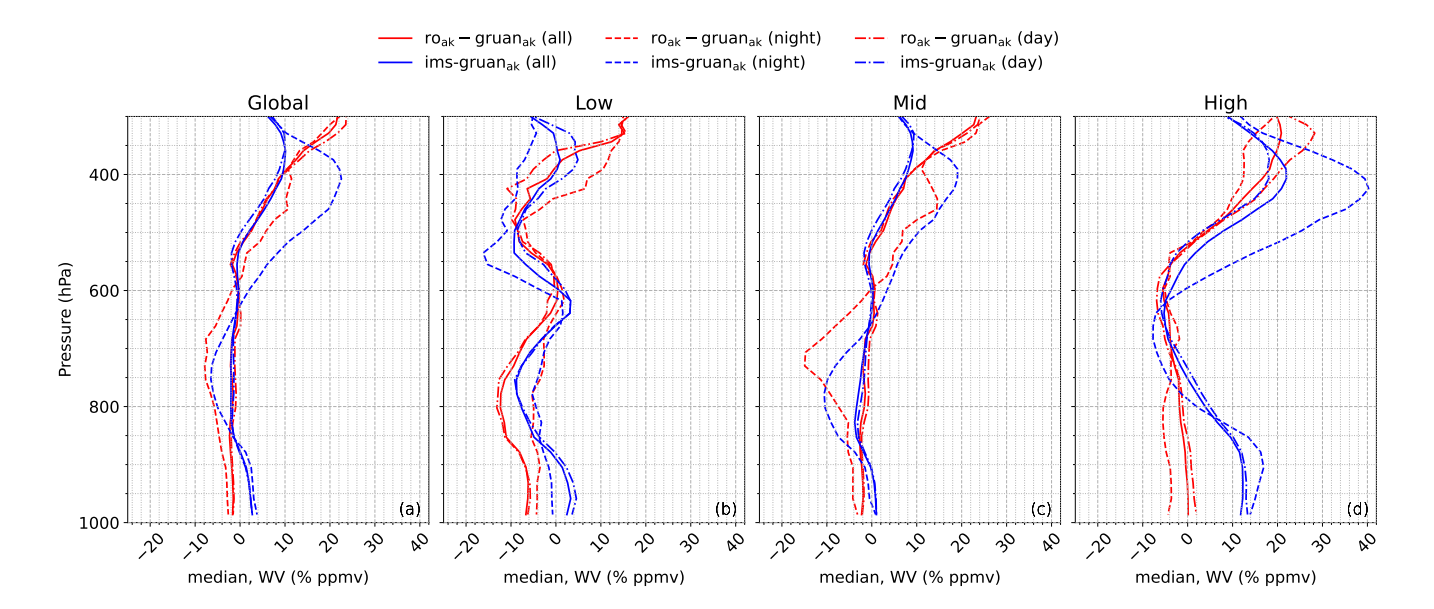


Figure 8. Median differences of RO and RAL IMS profiles to GRUAN WV profiles during day- and nighttime in (a) global, (b) low-, (c) mid-, and (d) high-latitude statistics. Solid lines represent the global set combining day and night matchups, dashed lines correspond to nighttime statistics, and dash-dotted lines correspond to daytime. Matchups follow CC1 and assume AK-smoothed RO and GRUAN profiles.

the lower mid troposphere in mid latitudes (RAL IMS, 10.59% ppmv; RO, 14.93% ppmv), and the moistest in the upper mid troposphere in high latitudes – where the RAL IMS wet bias peaks at 40.28% ppmv.

In UT, both data sets are wetter than GRUAN. RAL IMS shows a decreasing bias between 7.15% and 22.12% ppmv (driven mainly by high latitude statistics), whereas RO bias increases with altitude and ranges from 10.70% to 22.14% ppmv.

Figure 9 shows the MAD statistics.

A larger variability is observed in RAL IMS than in RO data in the lower troposphere – 20.24% and 14.15% ppmv, respectively. The pattern change around the lower mid troposphere, where the RO data shows more variability than RAL IMS – up to 44.18% and 38.28% ppmv, respectively. Most of this RO variability is observed in mid-latitudes.

Table 2 summarises the number of profiles part of the statistics using GRUAN as the reference.

An investigation of the influence of clouds in the statistics when using GRUAN as the reference, and same cloud scenarios as in Sect. 4.1.1, has also been performed. The evaluated cloud scenarios do not play a significant role in the biases observed in Fig. 6-9. Median and MAD figures are provided as supplementary material for reference.

375 5 Conclusions

370

This study presented the comparison based on 9.5 years of water vapour data retrieved from Metop-A satellite between June 2007 and December 2016. The vertical WV profiles were provided by two independent data sets, herein ROM SAF CDR v1.0



380



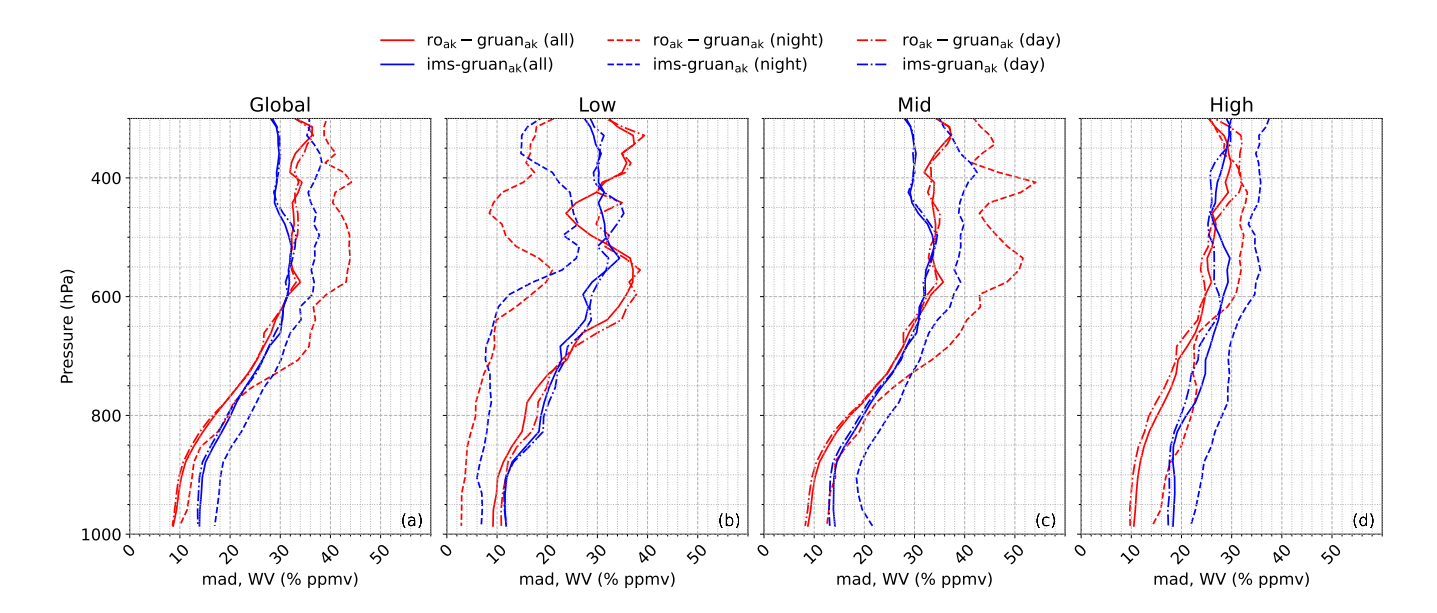


Figure 9. MAD of differences of RO and RAL IMS profiles to GRUAN WV profiles during day- and nighttime in (a) global, (b) low-, (c) mid-, and (d) high-latitude statistics. Solid lines represent the global set combining day and night matchups, dashed lines correspond to nighttime statistics, and dash-dotted lines correspond to daytime. Matchups follow CC1 and assume AK-smoothed RO and GRUAN profiles.

Table 2. Number of profiles part of the statistics using GRUAN as the reference. Numbers correspond to the largest number of points available at a given level, since they vary for different reasons – especially in the lower troposphere. "IMS*" refers to profiles that assume a 100-km collocation criterion.

	Global	Low	Mid	High
RO	3,258	288	1,530	1,440
IMS	89,593	1,828	73,700	14,065
IMS*	20,032	311	17,276	2,445
IMS, day	71,298	978	61,657	8,663
IMS, night	14,471	268	10,176	4,027

water vapour profiles acquired by the GRAS receiver and retrieved via the 1D-Var method, and the Infrared and Microwave Sounding (IMS) scheme applied to Infrared Atmospheric Sounding Interferometer (IASI), Advanced Microwave Sounding Unit (AMSU-A) and Microwave Humidity Sounder (MHS). The matchups were collected using a 3-hour and 300-km collocation criteria, and the analysis using ERA-Interim analysis and GRUAN WV profiles as the references. The comparison followed closely the methodology described in Trent et al. (2023). The conclusions are summarized as follows:

- In LT (1000-850 hPa), the RAL IMS wet bias (up to 3.8% ppmv) is present both in the comparison to GRUAN, in agreement with Trent et al., and to ERA-I (up to 5.5% ppmv). The wet bias is observed in mid latitudes (w.r.t. ERA-



390

395



- I) and high latitudes (w.r.t. ERA-I and GRUAN), and it is larger in profiles over water than land (w.r.t. ERA-I). The evaluated cloud parameter sets did not substantially influence the bias (w.r.t. ERA-I).
 - RO WV data is consistently drier than ERA-I (about 2.2% ppmv at maximum) between 1000-300 hPa, and it is also drier than GRUAN (up to 4.6% ppmv) in LT.
 - In the mid troposphere (850–400 hPa), RAL IMS is drier than ERA-I (about 11.4% ppmv), especially in the mid latitudes, with cloud contamination showing a wet contribution in the statistics (500–400 hPa) in high latitudes. Compared to GRUAN, RAL IMS showed a dry bias in the lower mid troposphere (850–600 hPa) in agreement with Trent et al. (2023) but with a greater magnitude (up to 2.3% ppmv). In contrast, RAL IMS is wetter than GRUAN in the upper mid troposphere (600–400 hPa), by 22.5% ppmv.
 - In the upper troposphere (400−300 hPa), RAL IMS data is on average drier than ERA-I (11.4% ppmv) due to profiles in low and mid latitudes, but it is wetter than GRUAN in high latitudes.
 - RO WV data in drier than ERA-I in the mid and upper troposphere, mostly in low and mid latitudes. In the upper troposphere, RO tends to its background due to the assumptions considered in the 1D-Var retrieval (see Fig. 1).
 - Compared to GRUAN, a wet bias, up to 20% at 300 hPa, is observed in the RO WV median.
- Convoluting ERA-I and GRUAN profiles with RAL IMS AKs tends to make the smoothed profiles drier than their
 originals, and tends to reduce and to some extent equalise the mean difference deviation (MAD).
 - The comparable levels of agreement for IMS and RO with independent GRUAN profiles once AKs are accounted for in the interval between 400 and 850 hPa indicates their complementary attributes, i.e., dense spatial sampling and moderate vertical resolution (RAL IMS) cf. high vertical resolution and sparse spatial sampling (RO), could potentially be exploited in development of CDRs.
- The comparisons conducted on a common basis of RAL IMS and RO WV data with ERA-I and GRUAN contribute to their characterisation and validation against product requirements, which are essential tasks supporting their applications as CDRs. It also provides a reference point for future reprocessing campaigns of IMS and RO data, e.g., the upcoming ROM SAF CDR v2.0.

Appendix A: Conversion between mass and volume mixing ratio

410 The masses of water vapour and dry air are defined as

$$\varrho_{\rm w} = M_{\rm w} \frac{\rho_{\rm w}}{RT},\tag{A1}$$

$$\varrho_{\rm d} = M_{\rm d} \frac{\rho_{\rm d}}{RT},\tag{A2}$$





where M is the molar mass (kg/mol), ρ is the density (kg/m³), R is the gas constant (J/kg·K), and T is temperature (K). The specific humidity is

415
$$q = \frac{\varrho_{\rm w}}{\varrho_{\rm w} + \varrho_{\rm d}} = \frac{\rho_{\rm w}}{\rho_{\rm d}/\varepsilon + \rho_{\rm w}},$$
 (A3)

where $\varepsilon = M_{\rm w}/M_{\rm d} \approx 0.622$. Mass mixing ratio is the ratio between the water vapour mass and the dry air,

$$MMR = \frac{\varrho_{W}}{\varrho_{d}} = \varepsilon \frac{\rho_{W}}{\rho_{d}} = \varepsilon VMR, \tag{A4}$$

where VMR is the volume mixing ratio, and so

$$\rho_{\rm w} = \rho_{\rm d} \, {\rm VMR},$$
 (A5)

420
$$\rho_{\rm d} = \rho_{\rm w}/{\rm VMR}$$
. (A6)

Substituting (A5) and (A6) into (A3),

$$q = \frac{\rho_{\rm d} \, \text{VMR}}{\rho_{\rm d} / \varepsilon + \rho_{\rm d} \, \text{VMR}} = \frac{\varepsilon \, \text{VMR}}{1 + \varepsilon \, \text{VMR}} = \frac{\text{MMR}}{1 + \text{MMR}}. \tag{A7}$$

Thus

$$MMR = \frac{q}{1-a},\tag{A8}$$

and water vapour in parts per million by volume (ppmv), i.e., VMR, is achieved by multiplying MMR by a factor of 1×10^6 (ppm) in (A4).

Appendix B: Conversion between relative humidity and mass mixing ratio

The mass mixing ratio can also be defined as

$$MMR = \varepsilon \frac{e}{p - e}, \tag{B1}$$

430 where e is the water vapour pressure (Pa) and p is the total pressure (Pa). The mass mixing ratio can be rewritten in terms of the relative humidity (RH, %),

$$MMR = \varepsilon \frac{RH e'}{p - RH e'},$$
(B2)

where e' is the water vapour partial pressure (Pa) given by (Hyland and Wexler, 1983)

$$e' = \exp\left(\sum_{i=-1}^{3} c_i T^i + c_4 \ln T\right),$$
 (B3)

where T is temperature (K) and $c_1 = -0.58002206 \times 10^4$, $c_0 = 0.13914993 \times 10^1$, $c_1 = -0.48640239 \times 10^{-1}$, $c_2 = 0.41764768 \times 10^{-4}$, $c_3 = -0.14452093 \times 10^{-7}$ and $c_4 = 0.65459673 \times 10^1$. Equation (B3) is defined for liquid water, i.e., $273.15 \le T \le 473.15$, and it is conventionally used by the GRUAN community throughout the troposphere (Miloshevich et al., 2006).

Finally, MMR can be used to calculate specific humidity or VMR (ppmv) as shown in Appendix A.



450



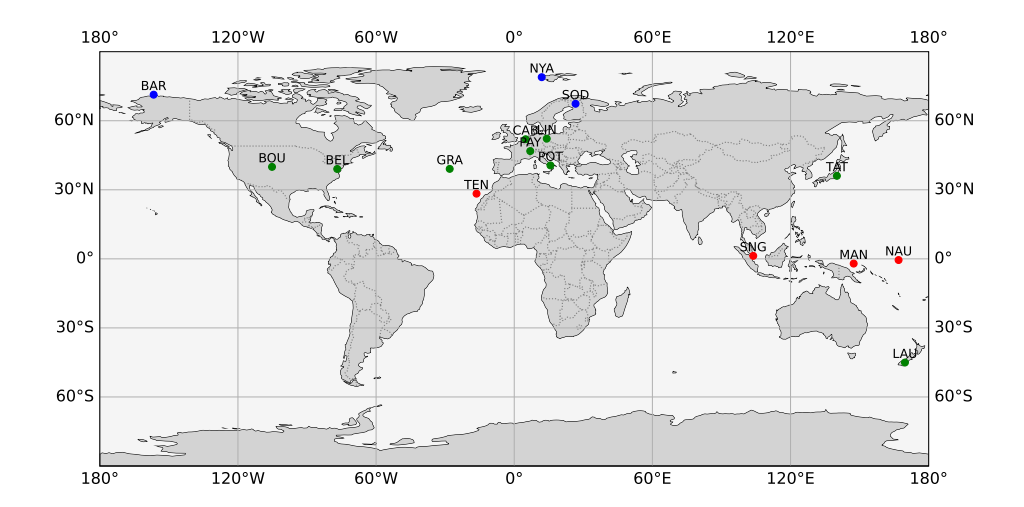


Figure C1. GRUAN sites considered in the comparison study. Red, green, and blue dots indicate low, mid, and high latitude sites.

Appendix C: GRUAN sites information

Figure C1 shows the location of GRUAN sites whose data were used as reference in the comparison between RAL IMS and RO WV data.

Table C1 lists further details about these stations. In comparison to (Trent et al., 2023), Data from SGP (Lamont, OK, USA) and REU (La Réunion, France) were not used in this study, whereas SNG (Singapore, Singapore) has been included.

Code availability. The code used in this comparison study, which performs the search for matchups, quality control, AK filtering and interpolation of profiles, and computes the statistics is available from the contact author upon request.

Data availability. RAL IMS temperature, water vapour, ozone and surface spectral emissivity data set is archived at Centre for Environmental Data Analysis (CEDA), https://doi.org/10.5285/489e9b2a0abd43a491d5afdd0d97c1a4 (last access: 30 October 2025). GRAS-RO specific humidity, part of Level 2B product, processed by ROM SAF using 1D-Var is available at https://doi.org/10.15770/EUM_SAF_GRM_0002 (last access: 30 October 2025). RS92 GRUAN Data Product Version 2, including relative humidity data, is available at https://www.gruan.org/data/data-products/gdp/rs92-gdp-2 (last access: 30 October 2025). The data underlying the results of this comparison study, i.e., data set of RAL IMS and GRAS-RO, and RAL IMS, GRAS-RO and GRUAN matchups, are available from the contact author upon request.

Author contributions. JN and KB were responsible for the conceptualisation of work packages and grant acquisition leading to this publication. VB, JN designed the methodology with inputs from BK, RS and TT. VB developed codes relate to data curation, performed the





Table C1. Description of GRUAN sites used in the comparison study. "Share" corresponds to the contribution of a given station to the data set of matchups. Source: https://www.gruan.org/network/sites.

Code	Name	Latitude	Longitude	Altitude	Share (%)
BAR	Barrow, AK, USA	71.32°	-156.61°	8 m	9.28
BEL	Beltsville, MD, USA	39.05°	-76.88°	53 m	0.01
BOU	Boulder, CO, USA	39.95°	-105.20°	1743 m	0.11
CAB	Cabauw, Netherlands	51.97°	4.92°	1 m	0.64
GRA	Graciosa, Portugal	39.09°	-28.03°	30 m	0.18
LAU	Lauder, New Zealand	-45.05°	169.68°	370 m	0.69
LIN	Lindenberg, Germany	52.21°	14.12°	98 m	72.07
MAN	Manus, Papua New Guinea	-2.06°	147.42°	6 m	0.10
NAU	Nauru, Nauru	-0.52°	166.92°	7 m	0.12
NYA	Ny-Ålesund, Norway	78.92°	11.93°	5 m	5.81
PAY	Payerne, Switzerland	46.81°	6.95°	491 m	0.35
POT	Potenza, Italy	40.60°	15.72°	720 m	0.06
SNG	Singapore, Singapore	1.30°	103.80°	21 m	0.13
SOD	Sodankylä, Finland	67.37°	26.63°	179 m	2.29
TAT	Tateno, Japan	36.06°	140.13°	27 m	6.24
TEN	Tenerife, Spain	28.32°	-16.38°	115 m	1.92

investigation, formal analysis and visualisations, under the supervision of JN and KN. VB prepared the original draft with contributions from 455 JN and BK. All authors contributed to the discussion of results and review of the manuscript.

Competing interests. The contact author has declared that none of the authors has any competing interests.

Acknowledgements. This study was funded by European Space Agency (ESA), contract no. 4000123554/18/I-NB, via the Water Vapour Climate Change Initiative (WV_cci) project (https://climate.esa.int/en/projects/water-vapour/), Phase 2.





References

- Bodeker, G. E., Bojinski, S., Cimini, D., Dirksen, R. J., Haeffelin, M., Hannigan, J. W., Hurst, D. F., Leblanc, T., Madonna, F., Maturilli, M., Mikalsen, A. C., Philipona, R., Reale, T., Seidel, D. J., Tan, D. G. H., Thorne, P. W., Vömel, H., and Wang, J.: Reference Upper-Air Observations for Climate: From Concept to Reality, Bulletin of the American Meteorological Society, 97, 123–135, https://doi.org/10.1175/BAMS-D-14-00072.1, 2016.
- Bojinski, S., Verstraete, M., Peterson, T. C., Richter, C., Simmons, A., and Zemp, M.: The Concept of Essential Climate Variables in Support of Climate Research, Applications, and Policy, Bulletin of the American Meteorological Society, 95, 1431–1443, https://doi.org/10.1175/BAMS-D-13-00047.1, 2014.
 - Culverwell, I. D., Lewis, H. W., Offiler, D., Marquardt, C., and Burrows, C. P.: The Radio Occultation Processing Package, ROPP, Atmos. Meas. Tech., 8, 1887–1899, https://doi.org/10.5194/amt-8-1887-2015, 2015.
- Dee, D. P., Uppala, S. M., Simmons, A. J., Berrisford, P., Poli, P., Kobayashi, S., Andrae, U., Balmaseda, M. A., Balsamo, G., Bauer,
 P., Bechtold, P., Beljaars, A. C. M., van de Berg, L., Bidlot, J., Bormann, N., Delsol, C., Dragani, R., Fuentes, M., Geer, A. J., Haimberger, L., Healy, S. B., Hersbach, H., Hólm, E. V., Isaksen, L., Kållberg, P., Köhler, M., Matricardi, M., McNally, A. P., Monge-Sanz, B. M., Morcrette, J.-J., Park, B.-K., Peubey, C., de Rosnay, P., Tavolato, C., Thépaut, J.-N., and Vitart, F.: The ERA-Interim reanalysis: configuration and performance of the data assimilation system, Quarterly Journal of the Royal Meteorological Society, 137, 553–597, https://doi.org/10.1002/qj.828, 2011.
- Dirksen, R. J., Sommer, M., Immler, F. J., Hurst, D. F., Kivi, R., and Vömel, H.: Reference quality upper-air measurements: GRUAN data processing for the Vaisala RS92 radiosonde, Atmospheric Measurement Techniques, 7, 4463–4490, https://doi.org/10.5194/amt-7-4463-2014, 2014.
 - Feltz, M. L., Knuteson, R. O., Revercomb, H. E., and Tobin, D. C.: A methodology for the validation of temperature profiles from hyperspectral infrared sounders using GPS radio occultation: Experience with AIRS and COSMIC, Journal of Geophysical Research: Atmospheres, 119, 1680–1691, https://doi.org/10.1002/2013JD020853, 2014.
 - Gilpin, S., Rieckh, T., and Anthes, R.: Reducing representativeness and sampling errors in radio occultation–radiosonde comparisons, Atmospheric Measurement Techniques, 11, 2567–2582, https://doi.org/10.5194/amt-11-2567-2018, 2018.
 - Gleisner, H., Lauritsen, K. B., Nielsen, J. K., and Syndergaard, S.: Evaluation of the 15-Year ROM SAF Monthly Mean GPS Radio Occultation Climate Data Record, Atmospheric Measurement Techniques, 13, 3081–3098, https://doi.org/10.5194/amt-13-3081-2020, 2020.
- Healy, S. B. and Eyre, J. R.: Retrieving Temperature, Water Vapour and Surface Pressure Information from Refractive-index Profiles Derived by Radio Occultation: A Simulation Study, Quarterly Journal of the Royal Meteorological Society, 126, 1661–1683, https://doi.org/10.1002/qj.49712656606, 2000.
 - Hilton, F., Armante, R., August, T., Barnet, C., Bouchard, A., Camy-Peyret, C., Capelle, V., Clarisse, L., Clerbaux, C., Coheur, P.-F., Collard, A., Crevoisier, C., Dufour, G., Edwards, D., Faijan, F., Fourrié, N., Gambacorta, A., Goldberg, M., Guidard, V., Hurtmans, D., Illingworth, S., Jacquinet-Husson, N., Kerzenmacher, T., Klaes, D., Lavanant, L., Masiello, G., Matricardi, M., McNally, A., Newman, S., Pavelin, E.,
- S., Jacquinet-Husson, N., Kerzenmacher, T., Klaes, D., Lavanant, L., Masiello, G., Matricardi, M., McNally, A., Newman, S., Pavelin, E., Payan, S., Péquignot, E., Peyridieu, S., Phulpin, T., Remedios, J., Schlüssel, P., Serio, C., Strow, L., Stubenrauch, C., Taylor, J., Tobin, D., Wolf, W., and Zhou, D.: Hyperspectral Earth Observation from IASI: Five Years of Accomplishments, Bulletin of the American Meteorological Society, 93, 347–370, https://doi.org/10.1175/BAMS-D-11-00027.1, 2012.



500



- Ho, S.-P., Kuo, Y.-H., and Sokolovskiy, S.: Improvement of the Temperature and Moisture Retrievals in the Lower Troposphere

 Using AIRS and GPS Radio Occultation Measurements, Journal of Atmospheric and Oceanic Technology, 24, 1726–1739, https://doi.org/10.1175/JTECH2071.1, 2007.
 - Ho, S.-p., Zhou, X., Kuo, Y.-H., Hunt, D., and Wang, J.-h.: Global Evaluation of Radiosonde Water Vapor Systematic Biases using GPS Radio Occultation from COSMIC and ECMWF Analysis, Remote Sensing, 2, 1320–1330, https://doi.org/10.3390/rs2051320, 2010.
 - Ho, S.-p., Kireev, S., Shao, X., Zhou, X., and Jing, X.: Processing and Validation of the STAR COSMIC-2 Temperature and Water Vapor Profiles in the Neutral Atmosphere, Remote Sensing, 14, 5588, https://doi.org/10.3390/rs14215588, 2022.
 - Holm, E. V. and Kral, T.: Flow-dependent, geographically varying background error covariances for 1D-VAR applications in MTG-IRS L2 Processing, ECMWF Technical Memorandum No. 680, 2012.
 - Hyland, R. W. and Wexler, A.: Formulations for the thermodynamic properties of the saturated phases of H2O from 173.15 K to 473.15 K, ASHRAE Trans., 89, 500–519, 1983.
- Klaes, K. D., Ackermann, J., Anderson, C., Andres, Y., August, T., Borde, R., Bojkov, B., Butenko, L., Cacciari, A., Coppens, D., Crapeau, M., Guedj, S., Hautecoeur, O., Hultberg, T., Lang, R., Linow, S., Marquardt, C., Munro, R., Pettirossi, C., Poli, G., Ticconi, F., Vandermarcq, O., Vasquez, M., and Vazquez-Navarro, M.: The EUMETSAT Polar System: 13+ Successful Years of Global Observations for Operational Weather Prediction and Climate Monitoring, Bulletin of the American Meteorological Society, 102, E1224–E1238, https://doi.org/10.1175/BAMS-D-20-0082.1, 2021.
- Kuo, Y.-H., Wee, T.-K., Sokolovskiy, S., Rocken, C., Schreiner, W., Hunt, D., and Anthes, R.: Inversion and Error Estimation of GPS Radio Occultation Data, Journal of the Meteorological Society of Japan, 82, 507–531, https://doi.org/10.2151/jmsj.2004.507, 2004.
 - Kursinski, E. R., Hajj, G. A., Schofield, J. T., Linfield, R. P., and Hardy, K. R.: Observing Earth's Atmosphere with Radio Occultation Measurements Using the Global Positioning System, Journal of Geophysical Research: Atmospheres, 102, 23429–23465, https://doi.org/10.1029/97JD01569, 1997.
- Ladstädter, F., Steiner, A. K., Schwärz, M., and Kirchengast, G.: Climate Intercomparison of GPS Radio Occultation, RS90/92 Radiosondes and GRUAN from 2002 to 2013, Atmospheric Measurement Techniques, 8, 1819–1834, https://doi.org/10.5194/amt-8-1819-2015, 2015.
 - Ladstädter, F.: Collocating GRAS with nadir sounders onboard of Metop: An assessment for instrument and climate monitoring, Tech. Rep. SAF/GRAS/DMI/REP/VS07/001, VS7, EUMETSAT ROM SAF, https://rom-saf.eumetsat.int/Publications/reports/grassaf_vs07_rep_v11.pdf, 2012.
- Li, J., Wolf, W. W., Menzel, W. P., Zhang, W., Huang, H.-L., and Achtor, T. H.: Global Soundings of the Atmosphere from ATOVS Measurements: The Algorithm and Validation, Journal of Applied Meteorology, 39, 1248–1268, https://doi.org/10.1175/1520-0450(2000)039<1248:GSOTAF>2.0.CO;2, 2000.
 - Li, Y., Yuan, Y., and Wang, X.: Assessments of the Retrieval of Atmospheric Profiles from GNSS Radio Occultation Data in Moist Tropospheric Conditions Using Radiosonde Data, Remote Sensing, 12, 2717, https://doi.org/10.3390/rs12172717, 2020.
- Liu, C.-Y., Li, J., Ho, S.-P., Liu, G.-R., Lin, T.-H., and Young, C.-C.: Retrieval of Atmospheric Thermodynamic State From Synergistic Use of Radio Occultation and Hyperspectral Infrared Radiances Observations, IEEE Journal of Selected Topics in Applied Earth Observations and Remote Sensing, 9, 744–756, https://doi.org/10.1109/JSTARS.2015.2444274, 2016.
 - Meredith, A., Leroy, S., Halperin, L., and Cahoy, K.: Efficient collocation of global navigation satellite system radio occultation soundings with passive nadir microwave soundings, Atmospheric Measurement Techniques, 16, 3345–3361, https://doi.org/10.5194/amt-16-3345-2023, 2023.





- Miloshevich, L. M., Vömel, H., Whiteman, D. N., Lesht, B. M., Schmidlin, F. J., and Russo, F.: Absolute Accuracy of Water Vapor Measurements from Six Operational Radiosonde Types Launched during AWEX-G and Implications for AIRS Validation, Journal of Geophysical Research: Atmospheres, 111, 2005JD006 083, https://doi.org/10.1029/2005JD006083, 2006.
- Poli, P., Healy, S. B., and Dee, D. P.: Assimilation of Global Positioning System Radio Occultation Data in the ECMWF ERA–Interim Reanalysis, Quarterly Journal of the Royal Meteorological Society, 136, 1972–1990, https://doi.org/10.1002/qj.722, 2010.
 - Rieckh, T., Anthes, R., Randel, W., Ho, S.-P., and Foelsche, U.: Evaluating tropospheric humidity from GPS radio occultation, radiosonde, and AIRS from high-resolution time series, Atmospheric Measurement Techniques, 11, 3091–3109, https://doi.org/10.5194/amt-11-3091-2018, 2018.
- Rocken, C., Anthes, R., Exner, M., Hunt, D., Sokolovskiy, S., Ware, R., Gorbunov, M., Schreiner, W., Feng, D., Herman, B., Kuo, Y.-H., and Zou, X.: Analysis and Validation of GPS/MET Data in the Neutral Atmosphere, Journal of Geophysical Research: Atmospheres, 102, 29 849–29 866, https://doi.org/10.1029/97JD02400, 1997.
 - Rodgers, C. D. and Connor, B. J.: Intercomparison of remote sounding instruments, Journal of Geophysical Research: Atmospheres, 108, 2002JD002 299, https://doi.org/10.1029/2002JD002299, 2003.
- ROM SAF: ROM SAF Radio Occultation Climate Data Record Metop, EUMETSAT SAF on Radio Occultation Meteorology, https://doi.org/10.15770/EUM_SAF_GRM_0002, 2019.
 - ROM SAF: Algorithm Theoretical Baseline Document: Level 2B and 2C 1D-Var products, Tech. Rep. SAF/ROM/DMI/ALG/1DVAR/002, v4.3, EUMETSAT ROM SAF, https://rom-saf.eumetsat.int/product_documents/romsaf_atbd_1dvar.pdf, 2021.
 - ROM SAF: The Radio Occultation Processing Package (ROPP) input/output module user guide, Tech. Rep. SAF/ROM/ME-TO/UG/ROPP/002, v11.3, EUMETSAT ROM SAF, https://rom-saf.eumetsat.int/romsaf_ropp_ug_io.pdf, 2024.
- Schröder, M., Lockhoff, M., Fell, F., Forsythe, J., Trent, T., Bennartz, R., Borbas, E., Bosilovich, M. G., Castelli, E., Hersbach, H., Kachi, M., Kobayashi, S., Kursinski, E. R., Loyola, D., Mears, C., Preusker, R., Rossow, W. B., and Saha, S.: The GEWEX Water Vapor Assessment archive of water vapour products from satellite observations and reanalyses, Earth System Science Data, 10, 1093–1117, https://doi.org/10.5194/essd-10-1093-2018, 2018.
- Seidel, D. J., Berger, F. H., Diamond, H. J., Dykema, J., Goodrich, D., Immler, F., Murray, W., Peterson, T., Sisterson, D., Sommer, M.,

 Thorne, P., Vomel, H., and Wang, J.: Reference Upper-Air Observations for Climate: Rationale, Progress, and Plans, Bulletin of the

 American Meteorological Society, 90, 361–369, https://doi.org/10.1175/2008BAMS2540.1, 2009.
 - Sherwood, S. C., Roca, R., Weckwerth, T. M., and Andronova, N. G.: Tropospheric Water Vapor, Convection, and Climate, Reviews of Geophysics, 48, RG2001, https://doi.org/10.1029/2009RG000301, 2010.
- Siddans, R.: Algorithm Theoretical Baseline Document Part 2 IMS L2 Product, Tech. Rep. 2.0, ESA/ECSAT, https://climate.esa.int/en/projects/water-vapour, 2023.
 - Siddans, R., Gerber, D., and Bell, B.: Optimal Estimation Method retrievals with IASI, AMSU and MHS measurements, Tech. Rep. EUM/-CO/13/46000001252/THH, RAL Space, STFC Rutherford Appleton Laboratory, Harwell Oxford, 2015.
 - Siddans, R., Walker, J., Latter, B., Kerridge, B., Gerber, D., and Knappett, D.: RAL Infrared Microwave Sounder (IMS) temperature, water vapour, ozone and surface spectral emissivity. Centre for Environmental Data Analysis, v2.1, https://doi.org/10.5285/489e9b2a0abd43a491d5afdd0d97c1a4, 2018.
 - Sommer, M., Dirksen, R., and Immler, F.: RS92 GRUAN Data Product (RS92-GDP), Version 2, GRUAN Lead Centre (Deutscher Wetterdienst), https://doi.org/10.5676/GRUAN/RS92-GDP.2, 2012.



595



- Steiner, A. K., Ladstädter, F., Ao, C. O., Gleisner, H., Ho, S.-P., Hunt, D., Schmidt, T., Foelsche, U., Kirchengast, G., Kuo, Y.-H., Lauritsen, K. B., Mannucci, A. J., Nielsen, J. K., Schreiner, W., Schwärz, M., Sokolovskiy, S., Syndergaard, S., and Wickert, J.: Consistency and Structural Uncertainty of Multi-Mission GPS Radio Occultation Records, Atmospheric Measurement Techniques, 13, 2547–2575, https://doi.org/10.5194/amt-13-2547-2020, 2020.
 - Sun, B., Reale, A., Seidel, D. J., and Hunt, D. C.: Comparing Radiosonde and COSMIC Atmospheric Profile Data to Quantify Differences among Radiosonde Types and the Effects of Imperfect Collocation on Comparison Statistics, Journal of Geophysical Research: Atmospheres, 115, 2010JD014457, https://doi.org/10.1029/2010JD014457, 2010.
- 575 Susskind, J., Barnet, C., and Blaisdell, J.: Retrieval of Atmospheric and Surface Parameters from AIRS/AMSU/HSB Data in the Presence of Clouds, IEEE Transactions on Geoscience and Remote Sensing, 41, 390–409, https://doi.org/10.1109/TGRS.2002.808236, 2003.
 - Susskind, J., Barnet, C., Blaisdell, J., Iredell, L., Keita, F., Kouvaris, L., Molnar, G., and Chahine, M.: Accuracy of Geophysical Parameters Derived from Atmospheric Infrared Sounder/Advanced Microwave Sounding Unit as a Function of Fractional Cloud Cover, Journal of Geophysical Research: Atmospheres, 111, https://doi.org/10.1029/2005jd006272, 2006.
- 580 Todd, K.: toddkarin/global-land-mask: Release of version 1.0.0 (v1.0.0), Zenodo, https://doi.org/10.5281/zenodo.4066722, 2020.
 - Trent, T., Siddans, R., Kerridge, B., Schröder, M., Scott, N. A., and Remedios, J.: Evaluation of tropospheric water vapour and temperature profiles retrieved from MetOp-A by the Infrared and Microwave Sounding scheme, Atmospheric Measurement Techniques, 16, 1503–1526, https://doi.org/10.5194/amt-16-1503-2023, 2023.
- Vergados, P., Mannucci, A. J., and Ao, C. O.: Assessing the performance of GPS radio occultation measurements in retrieving tropospheric humidity in cloudiness: A comparison study with radiosondes, ERA-Interim, and AIRS data sets: GPS TROPOSPHERIC HUMIDITY, Journal of Geophysical Research: Atmospheres, 119, 7718–7731, https://doi.org/10.1002/2013JD021398, 2014.
 - Vergados, P., Mannucci, A. J., Ao, C. O., Verkhoglyadova, O., and Iijima, B.: Comparisons of the tropospheric specific humidity from GPS radio occultations with ERA-Interim, NASA MERRA, and AIRS data, Atmospheric Measurement Techniques, 11, 1193–1206, https://doi.org/10.5194/amt-11-1193-2018, 2018.
- Vömel, H., Selkirk, H., Miloshevich, L., Valverde-Canossa, J., Valdés, J., Kyrö, E., Kivi, R., Stolz, W., Peng, G., and Diaz, J. A.: Radiation Dry Bias of the Vaisala RS92 Humidity Sensor, Journal of Atmospheric and Oceanic Technology, 24, 953–963, https://doi.org/10.1175/JTECH2019.1, 2007.
 - Von Engeln, A., Bühler, S., Kirchengast, G., and Künzi, K.: Temperature profile retrieval from surface to mesopause by combining GNSS Radio Occultation and Passive Microwave Limb Sounder Data, Geophysical Research Letters, 28, 775–778, https://doi.org/10.1029/2000GL011718, 2001.
 - Wang, B.-R., Liu, X.-Y., and Wang, J.-K.: Assessment of COSMIC Radio Occultation Retrieval Product Using Global Radiosonde Data, Atmospheric Measurement Techniques, 6, 1073–1083, https://doi.org/10.5194/amt-6-1073-2013, 2013.
 - Wang, K.-N., Ao, C. O., Morris, M. G., Hajj, G. A., Kurowski, M. J., Turk, F. J., and Moore, A. W.: Joint 1DVar Retrievals of Tropospheric Temperature and Water Vapor from Global Navigation Satellite System Radio Occultation (GNSS-RO) and Microwave Radiometer Observations, Atmospheric Measurement Techniques, 17, 583–599, https://doi.org/10.5194/amt-17-583-2024, 2024.
 - Yang, S. and Zou, X.: Assessments of Cloud Liquid Water Contributions to GPS Radio Occultation Refractivity Using Measurements from COSMIC and CloudSat, Journal of Geophysical Research: Atmospheres, 117, 2011JD016452, https://doi.org/10.1029/2011JD016452, 2012.